Ocean Engineering 324 (2025) 120755

Contents lists available at ScienceDirect

Ocean Engineering

journal homepage: www.elsevier.com/locate/oceaneng

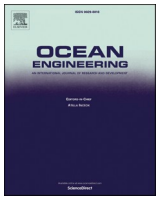

Research paper

Ensemble-Empirical-Mode-Decomposition (EEMD) on SWH prediction: The effect of decomposed IMFs, continuous prediction duration, and data-driven models

Yuanye Guo [a], Jicang Si [a,*], Yulian Wang [a], Farhan Hanif [b], Shuang Li [a], Mengwei Wu [a,**], Minyi Xu [a,***], Jianchun Mi [b]

[a] Dalian Key Lab of Marine Micro/Nano Energy and Self-Powered Systems, Marine Engineering College, Dalian Maritime University, Dalian, 116026, PR China
[b] College of Engineering, Peking University, Beijing, 100871, PR China

ARTICLE INFO

Keywords:
Significant wave height(SWH) prediction
Ensemble Empirical Mode Decomposition (EEMD)
Machine learning
IMF decomposition
Continuous prediction

ABSTRACT

This paper systematically investigates the impact of key factors on predicting significant wave height (SWH) using Ensemble Empirical Mode Decomposition (EEMD), specifically examining the number of decomposed Intrinsic Mode Functions (IMFs), the duration of continuous predictions, and the selection of data-driven models. Buoy data from Santa Monica Bay, California, is utilized. The findings reveal a significant improvement in prediction accuracy when EEMD is applied before using Support Vector Regression (SVR) and Artificial Neural Network (ANN) model, while improvements with Long Short-Term Memory (LSTM) networks are less pronounced. The study also determines the optimal number of intrinsic mode functions (IMFs) in EEMD decomposition necessary to balance predicting accuracy against computational cost, with RMSE values varying significantly based on the number of IMFs. Furthermore, the analysis indicates that increasing the length of continuous prediction steps leads to significant error accumulation, with the ANN model showing the slowest rate of error increase among the models tested. The results highlight the importance of optimizing model configurations to enhance predictive accuracy while managing computational demands.

1. Introduction

With the increase in global marine activities and their growing complexity, the accurate and rapid prediction of marine environmental parameters has become crucial for the success of marine engineering projects and safe navigation. The prediction and assessment of marine environmental parameters are becoming increasingly important for the implementation of marine engineering projects (Cornejo-Bueno et al., 2018) and the safety of navigation (Richter et al., 2017). Significant wave height (SWH), which describes the movement of ocean waves, is a vital environment parameter for engineering design and planning of the activities such as offshore oil and gas extraction (Graham, 1982), offshore wind power construction (Taylor and Jeon, 2018). Consequently, the accurate and reliable prediction of SWH has garnered extensive research attention (Jain and Deo, 2006; Mahjoobi et al., 2008; Özger et al., 2004).

However, the prediction of SWH is challenging due to the diverse factors that influence wave dynamics at different locations (Haver, 1986; Holthuijsen et al., 1989; Komen et al., 1984). Physical wave models like the third-generation WAM model (Group, 1988), the SWAN model for nearshore waves (Booij et al., 1999), and the WAVEWATCH III model (Tolman et al., 2002) are employed to simulate characteristics such as wave height, wavelength, and direction. These models consider numerous influences including wind speed and direction, seawater density, and seabed topography (Holthuijsen, 2010). However, they rely on extensive numerical simulations and substantial computational resources, which can delay processing times and fail to meet the need for prompt predictions (Wang et al., 2018).

Data-driven methods are some of the most effective for rapid and accurate predictions of wave heights (Deo and Jagdale, 2003; Makarynskyy, 2004). Advances in machine learning and artificial intelligence are continuously enhancing the reliability of predictive methods (Hanif et al., 2024a, 2024b). These methods leverage historical data to identify

* Corresponding author.
** Corresponding author.
*** Corresponding author.
E-mail addresses: sjc@dlmu.edu.cn (J. Si), wumengwei@dlmu.edu.cn (M. Wu), xuminyi@dlmu.edu.cn (M. Xu).

https://doi.org/10.1016/j.oceaneng.2025.120755
Received 12 September 2024; Received in revised form 18 January 2025; Accepted 20 February 2025
Available online 24 February 2025

Abbreviations

AI	Artificial Intelligence
ANN	Artificial Neural Network
AR	Autoregressive
ARIMA	Autoregressive Integrated Moving Average
ARMA	Autoregressive Moving Average
CEEMD	Complete Ensemble Empirical Mode Decomposition
CEEMDAN	Complete Ensemble Empirical Mode Decomposition with Adaptive Noise
EEMD	Ensemble Empirical Mode Decomposition
EOF	Empirical Orthogonal Function
EMD	Empirical Mode Decomposition
EWT	Empirical Wavelet Transform
GP	Genetic Programming
GRU	Gated Recurrent Unit
IMF	Intrinsic Mode Function
LR	Linear Regression
LMD	Local Mean Decomposition
LSTM	Long Short-Term Memory
MAE	Mean Absolute Error
MSE	Mean Squared Error
MWP	Mean Wave Period
NDBC	National Data Buoy Center
PACF	Partial Autocorrelation Function
RF	Random Forest
RMSE	Root Mean Square Error
SVM	Support Vector Machine
SVR	Support Vector Regression
SWAN	Simulating Waves Nearshore
SWH	Significant Wave Height
WAM	Wave Model
WD	Wavelet Decomposition

complex patterns in significant wave height (SWH) changes, enabling swift and precise forecasts. Soares et al. (1996) predicted the SWH series at two locations along the coast of Portugal using the Autoregressive (AR) model, noting its speed and lower resource demands compared to traditional wave simulations. Similarly, Agrawal and Deo (Agrawal and Deo, 2002) successfully implemented SWH prediction in an offshore area of India using Autoregressive Integrated Moving Average (ARIMA) and Autoregressive Moving Average (ARMA) models. Further developments have introduced more complex nonlinear machine learning models. Deo and Naidu (Deo and Naidu, 1998) demonstrated the effectiveness of ANNs for real-time predictions on India's east coast, and found that ANNs outperformed AR models in accuracy and reduced observational lag. Mahjoobi and Mosabbeb (Mahjoobi and Mosabbeb, 2009) found that Support Vector Machines (SVMs) with a Radial Basis Function kernel yielded better results than those with a Polynomial Function kernel, although they warned that underfitting could impair model performance. Additionally, Gaur and Deo (Gaur and Deo, 2008) explored Genetic Programming (GP) algorithm for long-term SWH prediction at two sites in the Gulf of Mexico, finding that GP-based models surpassed ANNs in accuracy. Malekmohamadi et al. (2011) investigated the use of several machine learning models, including SVMs, Bayesian Networks (BNs), ANNs, and Adaptive Neuro-Fuzzy Inference Systems (ANFIS) for predicting SWH on the western side of Lake Superior. Their findings indicated that SVMs, ANNs, and ANFIS delivered comparably accurate results, whereas BNs exhibited higher error rates. Subsequently, Sadeghifar et al. (2017) verified the application of Recurrent Neural Networks (RNNs) for SWH prediction, noting that RNNs are prone to issues with gradient vanishing and explosion. Addressing these limitations, Fan et al. (2020) employed Long Short-Term Memory (LSTM) networks, designed to avoid gradient instability, and found that LSTMs outperformed other models including ANNs, Extreme Learning Machines, and Random Forests in accuracy. Despite these advances, accurately predicting SWH remains challenging due to the data's multi-periodic and complex nonlinear characteristics (Janssen, 2008; Komen et al., 1996).

To increase the accuracy of SWH forecasting, preprocessing techniques such as decomposing time series data can be applied (Altunkaynak et al., 2023; Rasp et al., 2020). This method effectively separates periodic elements from complex time series, allowing for more precise predictions. Empirical Mode Decomposition (EMD), proposed by Huang et al. (1998), is a prominent technique applied to analyze nonlinear and non-stationary data. Duan et al. (2016a) combined EMD with the AR model to form the EMD-AR model, which outperformed the standalone AR model in significant wave height prediction. Duan et al. (2016b). Further combined EMD with SVR to propose the EMD-SVR hybrid prediction model. Compared with the single SVR model and the wavelet decomposition-based SVR model (WD-SVR), the significant wave height prediction results of the EMD-SVR model are more accurate. Additionally, Hao et al. (2022) developed an EMD-LSTM prediction model and applied it to forecast the significant wave heights of non-standing waves at different geographical locations off the coast of China. The study demonstrated that the EMD algorithm, by smoothing the time series of non-stationary waves, effectively suppressed errors caused by phase shifts, thereby significantly enhancing the prediction accuracy of the LSTM model. However, the EMD process can lead to mode mixing, where different intrinsic mode functions overlap, potentially reducing predictive accuracy (Wu and Huang, 2005).

To address the issue of mode mixing inherent in EMD, the Ensemble Empirical Mode Decomposition (EEMD) was proposed (Wu and Huang, 2009). This method enhances the decomposition process by adding Gaussian white noise to modifies the signal's extreme points. Ding et al. (2023) combined Empirical Orthogonal Function (EOF) analysis, EEMD, and Sample Convolutional Interaction Network (SCINet) to predict SWH and Mean Wave Period (MWP) in a region of the South China Sea. Six decomposition techniques—EMD, EEMD, Complete EEMD (CEEMD), CEEMD with Adaptive Noise (CEEMDAN), Empirical Wavelet Transform (EWT), and Local Mean Decomposition (LMD) were assessed, and EEMD was found to obtain the most accurate predictions. Song et al. (2023) developed an EEMD-LSTM model by combining EEMD with LSTM for SWH prediction in a region of the Indian Ocean, and found EEMD-LSTM outperformed Logistic Regression (LR), Random Forest (RF), LSTM, and Gated Recurrent Unit (GRU) models. Furthermore, Liu et al. (2017) introduced a novel approach using EEMD and X-band marine radar images to predict SWH. Their method significantly reduced the root mean square error compared to traditional signal-to-noise ratio-based methods and improved shadow-based methods, increasing accuracy with respect to buoy benchmarks by margins of 0.42 m and 0.12 m, respectively. FAN et al. studied the combination of different signal decomposition methods with the LSTM model and established several hybrid prediction models for semi-submersible short-term motion, namely EMD-LSTM, EEMD-LSTM, CEEMDAN-LSTM, and EWT-LSTM models. The results showed that the EWT-LSTM model achieved the lowest overall error, while the EEMD-LSTM model outperformed the EMD-LSTM model (Fan et al., 2023).

The number of IMFs generated during the EEMD process is crucial as it determines the level of decomposition of the original signal (Wu and Huang, 2010). Additionally, the duration of the prediction in hybrid models plays a significant role in continuous forecasting. Despite their importance, there appears to be limited systematic research on how these factors affect prediction accuracy.

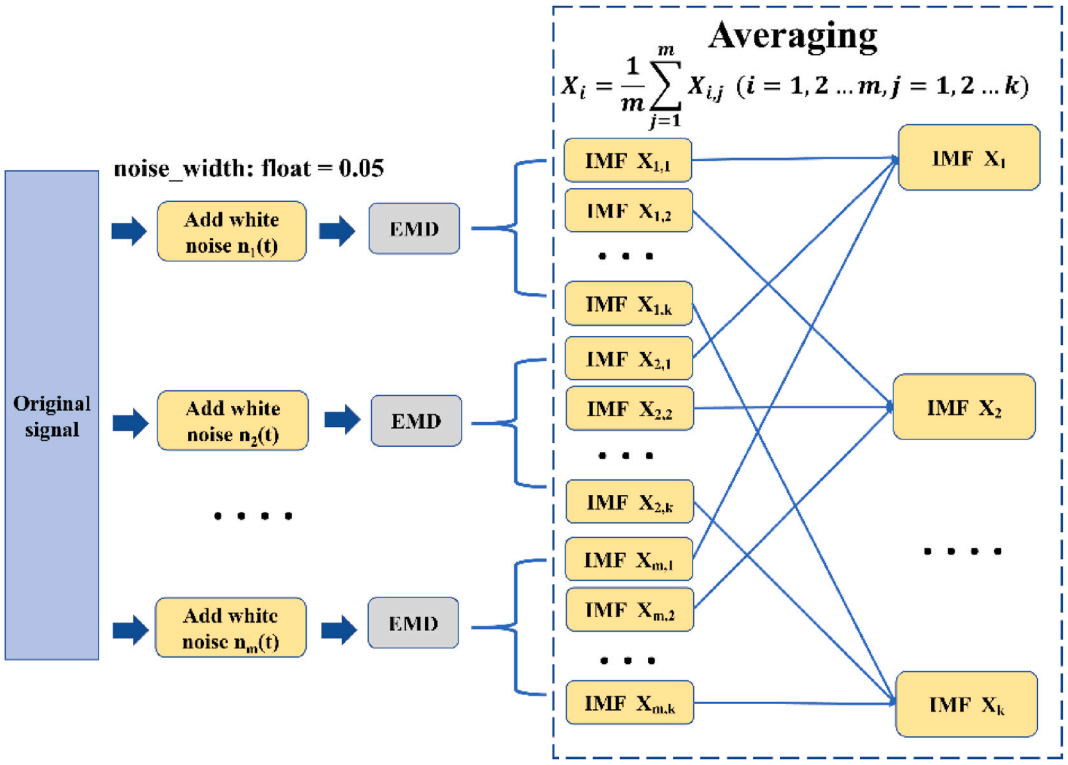

Fig. 1. Process of the EEMD method.

Therefore, the present work aims to address the above issue by investigating the effects of the number of IMFs and the length of the prediction window on SWH predictions using EEMD coupled with machine learning models. More specifically, this investigation will utilize those well-established machine learning techniques such as SVR, ANN, and LSTM networks as the prediction models. And the number of IMFs within the EEMD process under consistent prediction window durations to assess their impact on forecast accuracy will be discussed in detail. Subsequently, the length of the continuous prediction window will be changed to explore the model's effective prediction range.

The rest of this paper is organized as follows: Section 2 introduces the principles of the EEMD algorithm, SVR, ANN, and LSTM, along with model training and prediction methods, error metrics, and data sources; in Section 3, the prediction results are discussed and analyzed in some detail; finally, the concluding remarks are made in Section 4.

2. Models and mythologies

2.1. Ensemble Empirical Mode Decomposition (EEMD)

The Ensemble Empirical Mode Decomposition (EEMD) is an adaptive method for analyzing nonlinear and non-stationary signals (Huang et al., 1998). In the EEMD process, IMFs are extracted sequentially by identifying the local characteristics of the signal such as extrema and zero crossings. This enables the separation of signal components across different frequency ranges into distinct IMFs. However, challenges such as overlapping frequency components can lead to mode mixing, which compromises the clarity of these IMFs and affects further analysis and processing (Rilling et al., 2007; Yeh et al., 2010). To overcome this issue, the EEMD (Torres et al., 2011) introduces a method to mitigate mode mixing by adding steps to the EEMD process, as illustrated in Fig. 1:

(i) Introducing varying levels of Gaussian white noise to the original signal, creating multiple perturbed versions of the signal (e.g., $n_1(t)$, $n_2(t)$, etc.).
(ii) Independently performing EEMD on each perturbed signal, generating sets of IMFs (Xi,j) where 'i' denotes the IMF number, and 'j' refers to the sequence of extraction.
(iii) Averaging the IMFs from all perturbed signals to minimize the influence of the added noise, thereby refining the representation of the original signal's characteristics.

In this study, the EEMD was implemented using the PyEMD package in Python, setting the noise amplitude to 0.05 and limiting the maximum number of IMFs through specific parameter adjustments.

2.2. Support Vector Regression (SVR)

Support Vector Regression (SVR) is a specialized form of Support Vector Machines (SVM) employed in machine learning to minimize prediction errors within a specified margin (Cortes and Vapnik, 1995; Drucker et al., 1996).

First, the regression function is defined. In SVR, the input features x are mapped to a high-dimensional space through a nonlinear transformation. In this space, the goal is to find a hyperplane such that the difference between the predicted and actual values is minimized. The regression function is expressed as follows:

$$f(x) = w^T \varnothing(x) + b \tag{1}$$

where w is the weight vector of the regression hyperplane, $\varnothing(x)$ is the feature mapping function that uses a kernel to map the data into a high-dimensional space, and b is the bias term. To allow for some errors in the regression process, SVR introduces the tolerance ε, which limits the allowed error range in the regression model. Additionally, the slack variables ζ_i and ζ_i^* are introduced to handle samples whose errors exceed the tolerance ε:

$$y_i - \left(w^T \phi(x_i) + b\right) \le \varepsilon + \zeta_i \tag{2}$$

$$\left(w^T \phi(x_i) + b\right) - y_i \le \varepsilon + \zeta_i^* \tag{3}$$

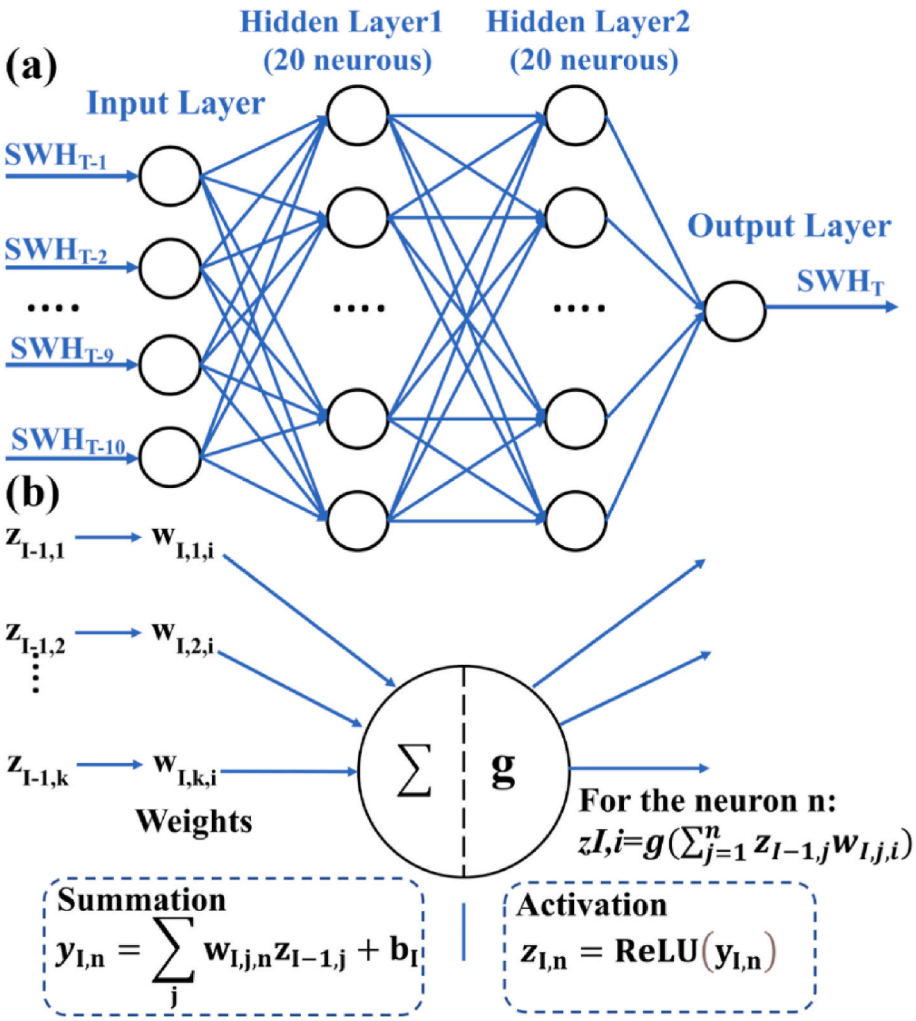

Fig. 2. (a) Schematic diagram of ANN in the present study and (b) computational process of hidden layer neurons in ANN.

$$\zeta_i, \zeta_i^* \geq 0, i = 1, \ldots, N \tag{4}$$

The subsequent step is the optimization objective. In regression tasks, SVR aims to find the optimal regression hyperplane by minimizing the following objective function. The objective is to maximize the smoothness of the regression hyperplane while balancing the trade-off between error minimization and model complexity:

$$min_{w,b,\zeta,\zeta^*} \frac{1}{2}\|w\|^2 + C\sum_{i=1}^{N}(\zeta_i + \zeta_i^*) \tag{5}$$

Where C is the regularization parameter, which controls the trade-off between training error and model complexity. The $\|w\|^2$ term represents the smoothness of the regression hyperplane; the smaller this value, the smoother the regression function.

Previous research by Mahjoobi and Mosabbeb (2009) demonstrated that SVR with an RBF kernel performs better in predicting SWH. This study was conducted using Python (version 3.9.18), implementing SVR from the Sklearn library with an RBF kernel. After tuning, the regularization parameter C was set to 1.0.

2.3. Artificial Neural Network (ANN)

ANN consists of numerous interconnected nodes, or neurons. In this study, a feedforward neural network architecture is employed. A feedforward neural network includes an input layer, several hidden layers, and an output layer. Each neuron in one layer is fully connected to all neurons in the preceding and succeeding layers, as illustrated in Fig. 2 (a). Training data enter the neural network through the input layer and undergo a series of linear and nonlinear transformations, resulting in the predicted output from the output layer (LeCun et al., 1998).

In the structure of a fully connected feedforward neural network, as illustrated in Fig. 2(b), the neurons n in the I-th hidden layer perform the following two steps of computation (McCulloch and Pitts, 1943):

(i) Summing the weighted inputs and introducing the bias term b_I for neurons in the previous layer (I−1 layer).

$$y_{I,n} = \sum_j w_{I,j,n} z_{I-1,j} + b_I \tag{6}$$

(ii) Applying a nonlinear transformation to $y_{I,n}$ to obtain the output of neuron n in the I-th layer.

$$z_{I,n} = g\left(y_{I,n}\right) \tag{7}$$

The training process of the ANN involves gradually adjusting the weights $w_{I,j,n}$ and biases b_I of each neuron to minimize the error between the ANN output and the target values of the training dataset $w_{I,j,n}$ represents the weight of neuron n in the I-th layer, and g(x) denotes the activation function.

In this study, the PyTorch framework (version 2.1.0) was utilized to train the ANN model, with GPU acceleration to enhance training speed.

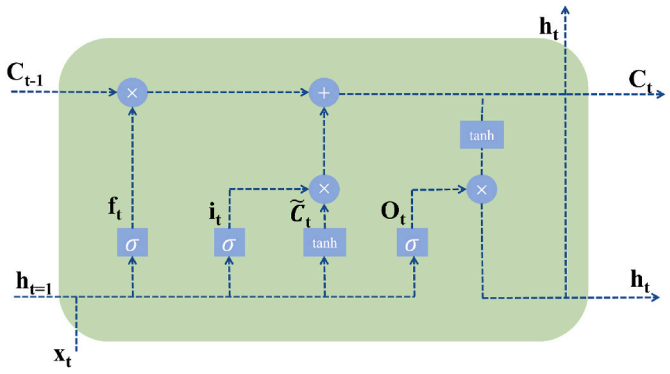

Fig. 3. The long short-term memory network unit architecture.

The neural network architecture consists of two hidden layers, each containing 20 neurons, and employs the ReLU activation function to mitigate the vanishing gradient problem (McCulloch and Pitts, 1943). The input layer comprises 10 nodes, and the output layer has 1 node, as illustrated in Fig. 2(a). The MSE is used as the loss function to calculate the difference between the model's output and the actual target values. The Adam algorithm (Kingma, 2014) is employed to train the model parameters, with a learning rate set at 0.001. Each model is trained for 2000 epochs to ensure thorough training and convergence. These parameters are selected by trail using the SWH data of buoy number 46221 for the first year.

2.4. Long Short-Term Memory (LSTM)

LSTM is an improved version of RNN(Hochreiter and Schmidhuber, 1997). It includes three integral components: the input gate, the forget gate, and the output gate (Hochreiter and Schmidhuber, 1997). Fig. 3 illustrates the internal structure of an LSTM unit. Here, f represents the forget gate, i represents the input gate, o represents the output gate, and h denotes the output. ht represents the current output, h_{t-1} represents the previous output, and x_t denotes the current input information. c_t signifies the memory cell state. The activation function used throughout is the hyperbolic tangent (tanh). The gates f, i, and o are computed using the sigmoid function, producing values in the range [0, 1].

In an LSTM unit, the process begins with the forget gate determining which information from the previous time step should be discarded. Next, the input gate selects new information to be added and generates a new memory component. The unit state is then updated by combining the information from the forget gate and the input gate. Finally, the output gate decides the output for the current time step.

The related calculations for an LSTM unit are as follows:

$$i_t = \sigma_i(W_i \times [h_{t-1}, x_t] + b_i) \tag{8}$$

$$f_t = \sigma\left(W_f \times [h_{t-1}, x_t] + b_f\right) \tag{9}$$

$$z_t = tan\, h(W_z \times [h_{t-1}, x_t] + b_z) \tag{10}$$

$$C_t = f \times C_{t-1} + i_t \times z_t \tag{11}$$

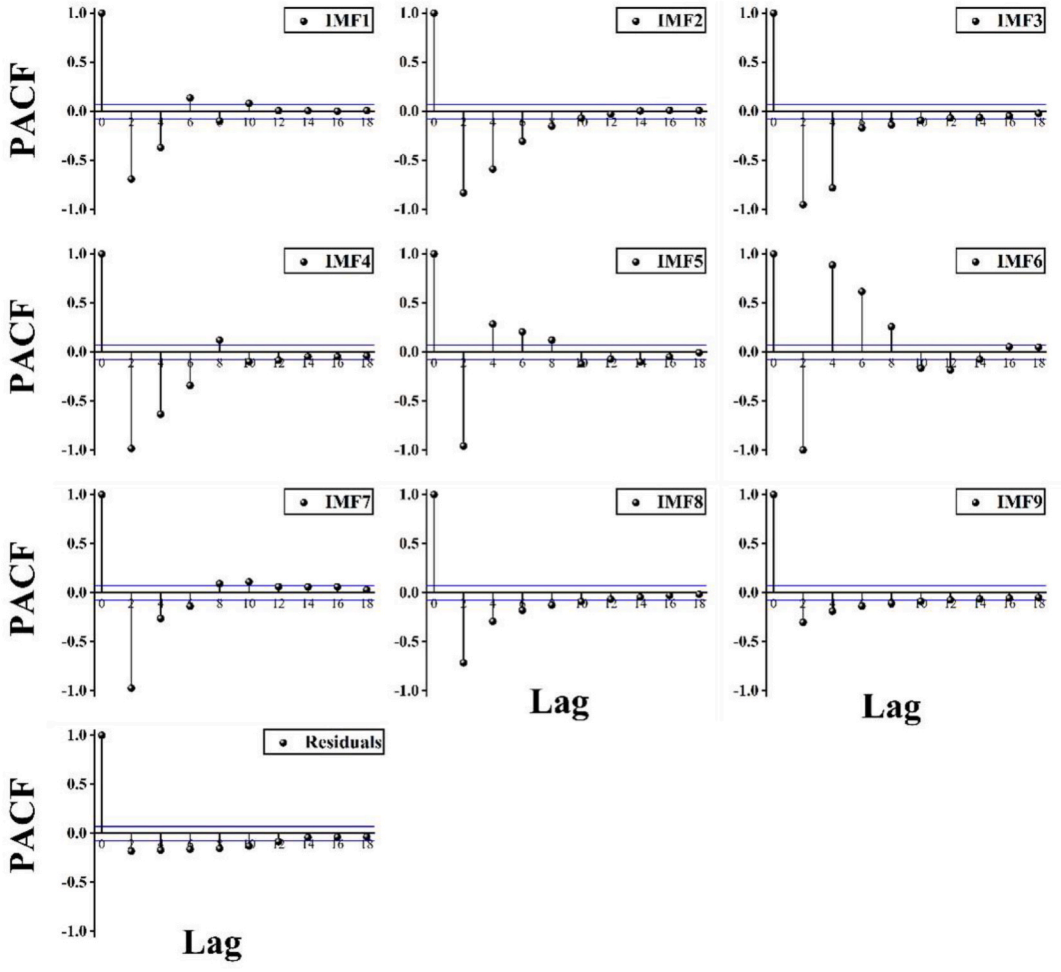

Fig. 4. Partial autocorrelation analysis for Buoy Point 46,221.

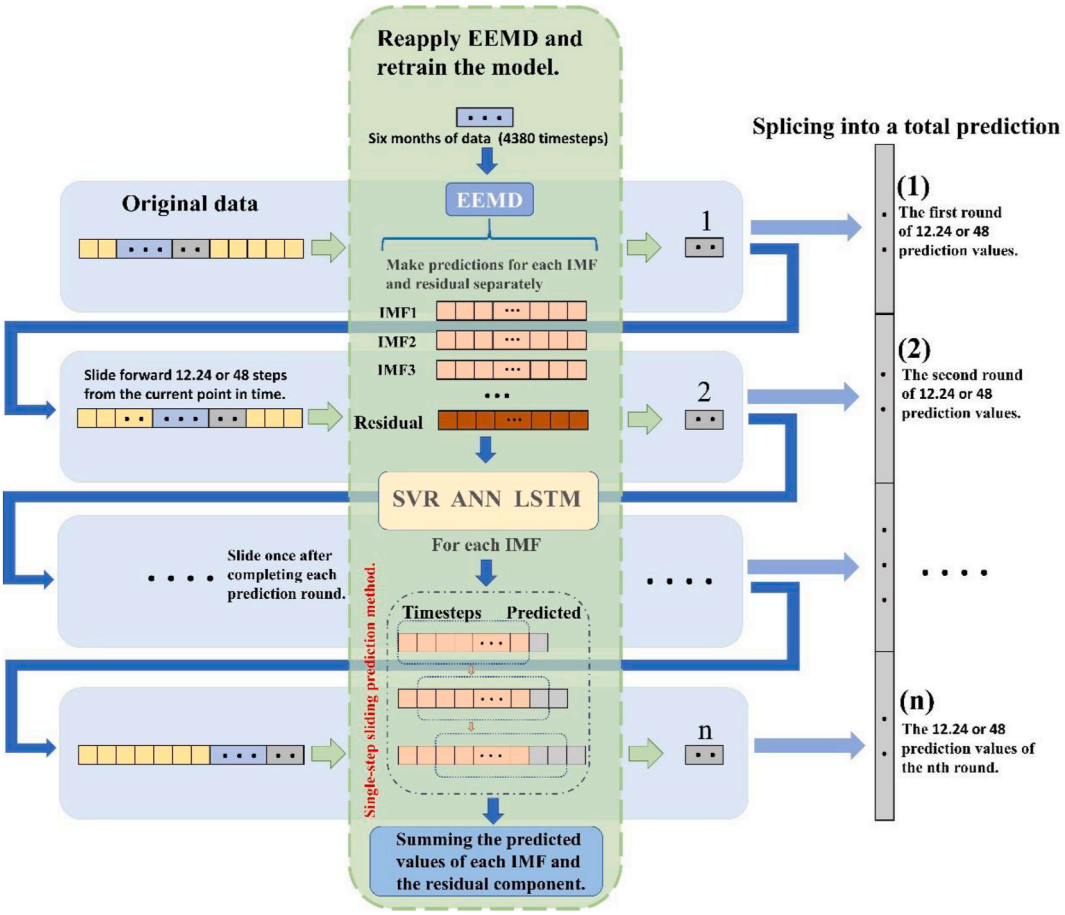

Fig. 5. Schematic diagram of sliding EEMD prediction.

$$O_t = \sigma(W_0 \times [h_{t-1}, x_t] + b_0) \tag{12}$$

$$h_t = O_t * tan\, h(C_t) \tag{13}$$

The weight matrices W_i, W_f, W_z, and W_o and the corresponding bias vectors b_i, b_f, b_z, and b_o are distinct. In this study, the LSTM model is constructed using PyTorch (version 2.1.0). Since the input data is a one-dimensional time series, the number of units in the input layer is set to 1. The hidden layer consists of 50 units, and because the prediction involves a single value, the output layer has 1 unit. To prevent overfitting, a dropout rate of 0.1 is applied. The loss function used is MSE, and the Adam optimizer is selected with a learning rate of 0.001. The model is trained for 2000 epochs.

2.5. Model training and prediction methods

In this research, we adopt a sliding EEMD prediction for consecutive prediction, as shown in Fig. 5. The sliding EEMD is realized by the following steps:

Applying partial autocorrelation validation to determine the relationship between the lag and residual components of each IMF and the current time series value (Ramsey, 1974). PACF analysis helps identify lag values in the time series that are directly correlated with the current value, determine the appropriate prediction step length, and reduce prediction errors.

Given the sliding nature of the EEMD method, the time series for each round of prediction varies. Therefore, the entire time series is subjected to partial autocorrelation analysis. For instance, at buoy point 46,221, PACF analysis is performed for each IMF component and residual item, as illustrated in Fig. 4. Based on the observations, a strategy is formulated to predict one step using every ten steps. Further analysis indicates that the accuracy of the prediction primarily relies on short-term data, and long-term data is not essential. Even when using only short-term data for training, reasonably accurate predictions can be obtained, while long-term data does not significantly improve the prediction performance.

The specific methodology is illustrated in Fig. 5:

(i) Data Extraction and EEMD Decomposition: A segment of SWH data is extracted from the original dataset, corresponding to the six months preceding the current time point (4380 data points). This historical data is then subjected to EEMD, resulting in multiple IMFs and a residual component.

(ii) Continuous Prediction Using Machine Learning Models: Various machine learning or artificial intelligence models, such as SVR, ANN, and LSTM, are applied to perform continuous prediction for each IMF and residual component. Predictions from the previous step are used as inputs for the subsequent step, and the results from all IMFs and residuals are summed to complete one sliding prediction cycle. Each time the window slides, retraining is required for each IMF.

(iii) Sliding Window Progression: The current time point is then moved backward by X steps (X = 12,24,48), and steps (i) and (ii) are repeated until the prediction process is complete

By employing the sliding EEMD strategy, the influence of future data on predictions is effectively minimized. Our experiments were conducted on a high-performance workstation equipped with an Intel® Core™ i9-14900K processor, featuring 24 cores and 32 threads, a base frequency of 3.2 GHz, 64 GB of RAM, and an NVIDIA GeForce RTX 3090 GPU.

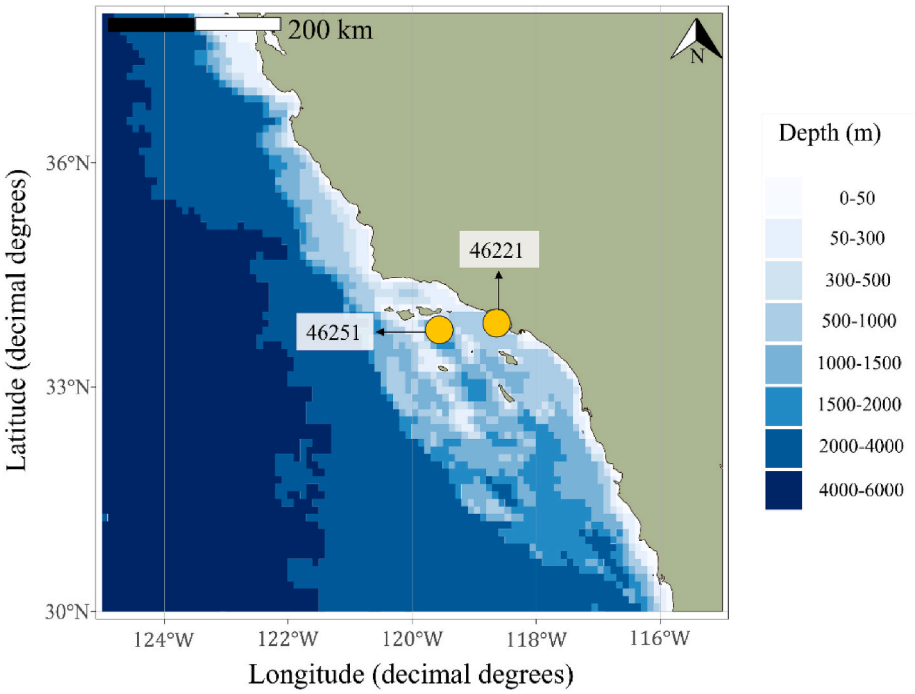

Fig. 6. Locations of the two buoy stations in Santa Monica bay.

Table 1
Detailed information for two buoy stations.

Buoy Station ID	Locations	Water Depth (m)	SWH (m)	Origin data	Complete data
NO.46221	33.860N 118.641 W	387	0.31–4.29	42,910	43,820
NO.46251	33.769N 119.565 W	1890	0.43–5.33	42,174	43,820

2.6. Error metrics

To compare the prediction performance of different hybrid models, we selected Root Mean Squared Error (RMSE), Mean Squared Error (MSE), and Mean Absolute Error (MAE) as evaluation metrics. These metrics measure the differences between predicted and actual observed values to assess model accuracy:

$$RMSE = \sqrt{\frac{1}{n}\sum_{i=1}^{n}(x_i - y_i)^2} \tag{14}$$

$$MSE = \frac{1}{n}\sum_{i=1}^{n}(x_i - y_i)^2 \tag{15}$$

$$MAE = \frac{1}{n}\sum_{i=1}^{n}|x_i - y_i| \tag{16}$$

Here, n is the number of samples, x_i is the actual value, and y_i is the corresponding predicted value. The smaller the values of RMSE, MSE, and MAE, the better the predictive capability of the model.

2.7. Data sources

In this research, we utilized buoy data from Santa Monica Bay, California, sourced from the National Data Buoy Center (NDBC). We specifically analyzed data from two buoy stations, one nearshore (46,221) and one offshore (46,251), selected for their comprehensive records of significant wave height (SWH) over a long-term period. The locations of these buoy stations are illustrated in Fig. 6.

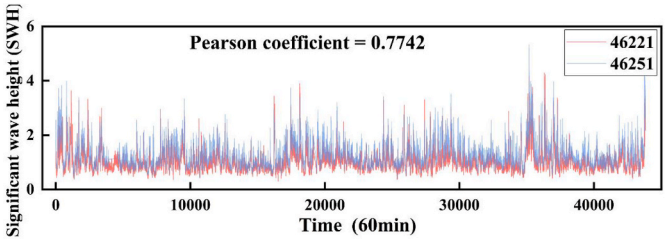

Fig. 7. Time Series of SWH at the Two buoy stations.

The dataset covers the period from January 2019 to December 2023, spanning five years. The model training is based on a six-month subset consisting of 4380 data entries, with a 60-min interval between data points. Table 1 provides detailed specifications of the two buoy stations. To address missing data, both datasets were subjected to linear interpolation, resulting in a complete dataset of 43,820 entries for each buoy. Subsequent analysis revealed that the offshore buoy 46,251 displayed more outliers and higher variability in SWH compared to its nearshore counterpart, buoy 46,221. The Pearson correlation coefficient between the wave height measurements at these two stations is 0.7742, as

Table 2
Prediction errors of single models and bybrid models with EEMD.

Station	Model	RMSE	MAE	MSE
46,221	SVR	0.3392	0.2469	0.1151
	ANN	0.2521	0.1693	0.0636
	LSTM	0.2590	0.1764	0.0671
	EEMD + SVR	0.2431	0.1673	0.0591
	EEMD + ANN	0.2149	0.1260	0.0462
	EEMD + LSTM	0.2381	0.1494	0.0567
46,251	SVR	0.3559	0.2746	0.1267
	ANN	0.3020	0.2111	0.0912
	LSTM	0.3074	0.2173	0.0945
	EEMD + SVR	0.2758	0.1942	0.0761
	EEMD + ANN	0.2478	0.1563	0.0614
	EEMD + LSTM	0.2604	0.1648	0.0678

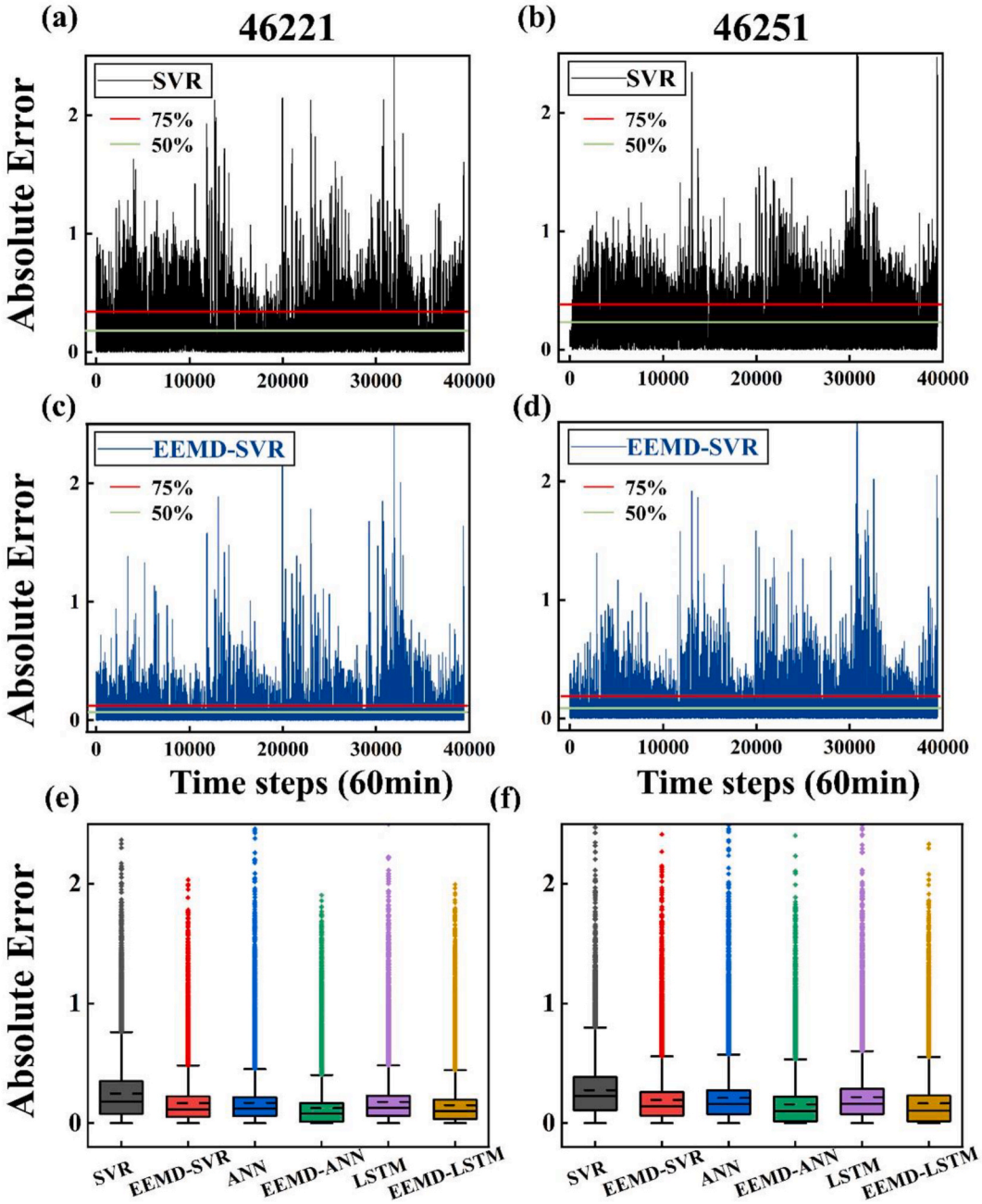

Fig. 8. Absolute error line charts for SVR at (a) buoy 46,221 and (b) buoy 46,251, and EEMD-SVR at (c) buoy 46,221 and (d) buoy 46,251, along with absolute error box plots for six prediction methods at (e) buoy 46,221 and (f) buoy 46,251.

illustrated in Fig. 7.

3. Results and discussion

3.1. Verification of the improved SWH prediction accuracy using EEMD

The present work evaluates the prediction accuracy of SWH sequences using various machine learning and artificial intelligence methods, including SVR, ANN, and LSTM models. These models were applied both with and without preprocessing by EEMD. A sliding window of 12 steps (equivalent to 12 h) was selected for continuous prediction, and EEMD was configured to produce three IMF. The prediction results for two measurement locations are summarized in Table 2.

The results demonstrate a significant improvement in prediction accuracy when EEMD preprocessing is applied. For example, at buoy point 46,221, the RMSE for the SVR model decreased from 0.3392 to 0.2431, representing a 28% reduction after applying EEMD. Additionally, the MAE and MSE decreased by 32% and 49%, respectively. For the ANN and LSTM models, preprocessing resulted in reductions in RMSE, MAE, and MSE by 15%, 26%, 27%, and 8%, 15%, 15%, respectively. Similar significant improvements were observed at buoy point 46,251, confirming that EEMD decomposition significantly enhances the prediction accuracy of various machine learning models for SWH sequences. Moreover, it is noteworthy that for machine learning models, the lower the model complexity, the more substantial the improvement in prediction results when EEMD is used for preprocessing. Specifically, the prediction performance of the EEMD-SVR model outperforms those of the ANN and LSTM models, offering new insights into the development of fast and lightweight prediction models.

Fig. 8 visually illustrates the reduction in absolute error for the SVR

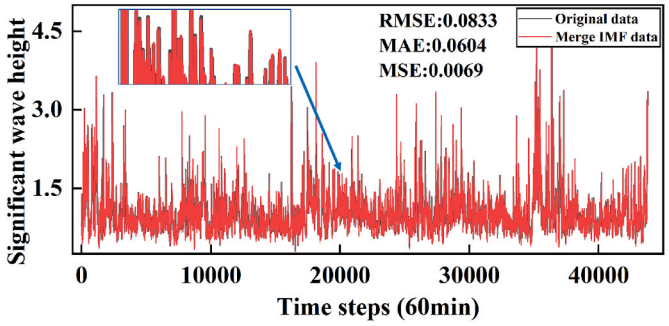

Fig. 9. Comparison between the signal reconstructed by summing the decomposed IMFs and the original signal.

model, both with and without EEMD preprocessing, using line charts and box plots. The predictions from the hybrid EEMD-SVR model are more closely aligned with the measured data and exhibit fewer outliers compared to the standard SVR model. Similar improvements are also observed in the ANN models and the LSTM models, as shown in Fig. 8(e) and (f). These enhancements suggest that EEMD effectively captures the varying patterns of the signal, thereby improving overall prediction accuracy. Although the single LSTM model demonstrates higher prediction accuracy than the single ANN model, the improvement after EEMD preprocessing is less pronounced in the LSTM model compared to the EEMD-ANN model. This could be due to the white noise introduced during the EEMD decomposition of the SWH data, which results in significant errors during the reconstruction of the signal post-decomposition. Given the robust learning capabilities of LSTM models, they are particularly sensitive to such random errors, which may explain the marginal improvement in prediction accuracy. Additionally, LSTM training typically requires a larger dataset, and using smaller input sizes may lead to underfitting. This suggests that when applying EEMD, careful consideration should be given to the complexity of the predictive model to avoid potential underfitting issues.

To further examine the impact of preprocessing, Fig. 9 compares the original SWH signal with its reconstruction post-EEMD decomposition. During decomposition, the EEMD algorithm decomposes the time series into three IMFs and one residual. Although the reconstructed signal closely matches the original signal's trend, the SWH reconstruction yields an RMSE of 0.0833, an MAE of 0.0604, and an MSE of 0.0069 (white noise is introduced with an amplitude of 0.05). These errors are considerable compared to the prediction errors in Table 2. This comparison suggests that while the addition of white noise in EEMD can help avoid mode mixing—a common issue in traditional EMD—it also introduces new errors. Therefore, optimizing the EEMD algorithm involves balancing the reduction of mode mixing against minimizing the impact on prediction accuracy.

The study also evaluates the prediction accuracy of various machine learning models across different months, using RMSE as the error metric. Fig. 10 displays radar charts that illustrate the monthly prediction errors for different models that underwent EEMD during the period from 2019 to 2023 at two observational points. At buoy point 46,221, the three methods of prediction reveal increased errors from June to November. Similarly, at buoy point 46,251, the errors remain relatively consistent from January through May but escalate in June and July. Referring to Fig. 7 for these locations, these months with elevated prediction errors coincide with periods of significant wave height fluctuations and the presence of more outliers. These conditions complicate the prediction process. Conversely, months yielding more precise predictions display more consistent wave height data. For months where prediction proves more challenging, exploring various model types and adjusting parameter settings may improve forecast accuracy.

3.2. Impact of decomposing different numbers of IMFs on accuracy of SWH prediction

The number of IMFs decomposed by EEMD is a crucial parameter, with each IMF representing features of the original signal at different scales and frequencies. Fig. 11 illustrates the influence of using different numbers of IMFs—3, 5, and 9—on the decomposition of training data through EEMD. The results highlight that altering the number of IMFs does not significantly impact the initial signal features, confirming the stability and robustness of the EEMD method. As the number of IMFs increases, the residual sequence stabilizes, displaying clear periodic patterns. If clear periodic or oscillatory features remain in the decomposed residuals, this indicates the potential to extract additional signals into more IMFs(Huang et al., 1998). However, the analysis reveals that when the number of IMFs reaches five, the residuals exhibit strong periodic characteristics that are often predictable by machine learning models, suggesting that additional decomposition may be unnecessary. This pattern underscores that increasing the number of IMFs does not necessarily improve machine learning training or prediction accuracy, emphasizing the importance of optimizing the balance between decomposition detail and computational efficiency.

Table 3 presents a comparison of prediction errors between the forecasted and actual SWH data, analyzing the impact of different numbers of decomposed IMFs on prediction accuracy. This analysis uses a sliding window approach with a continuous prediction step length of 12 time steps, equivalent to 12 h. The results indicate that an increase in

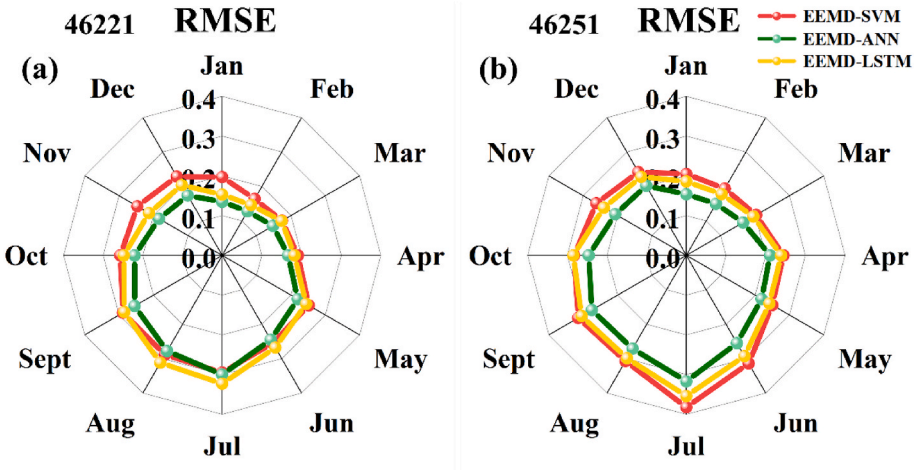

Fig. 10. Radar charts of RMSE for three prediction methods in different months at (a) buoy 46,221 and (b) buoy 46,251.

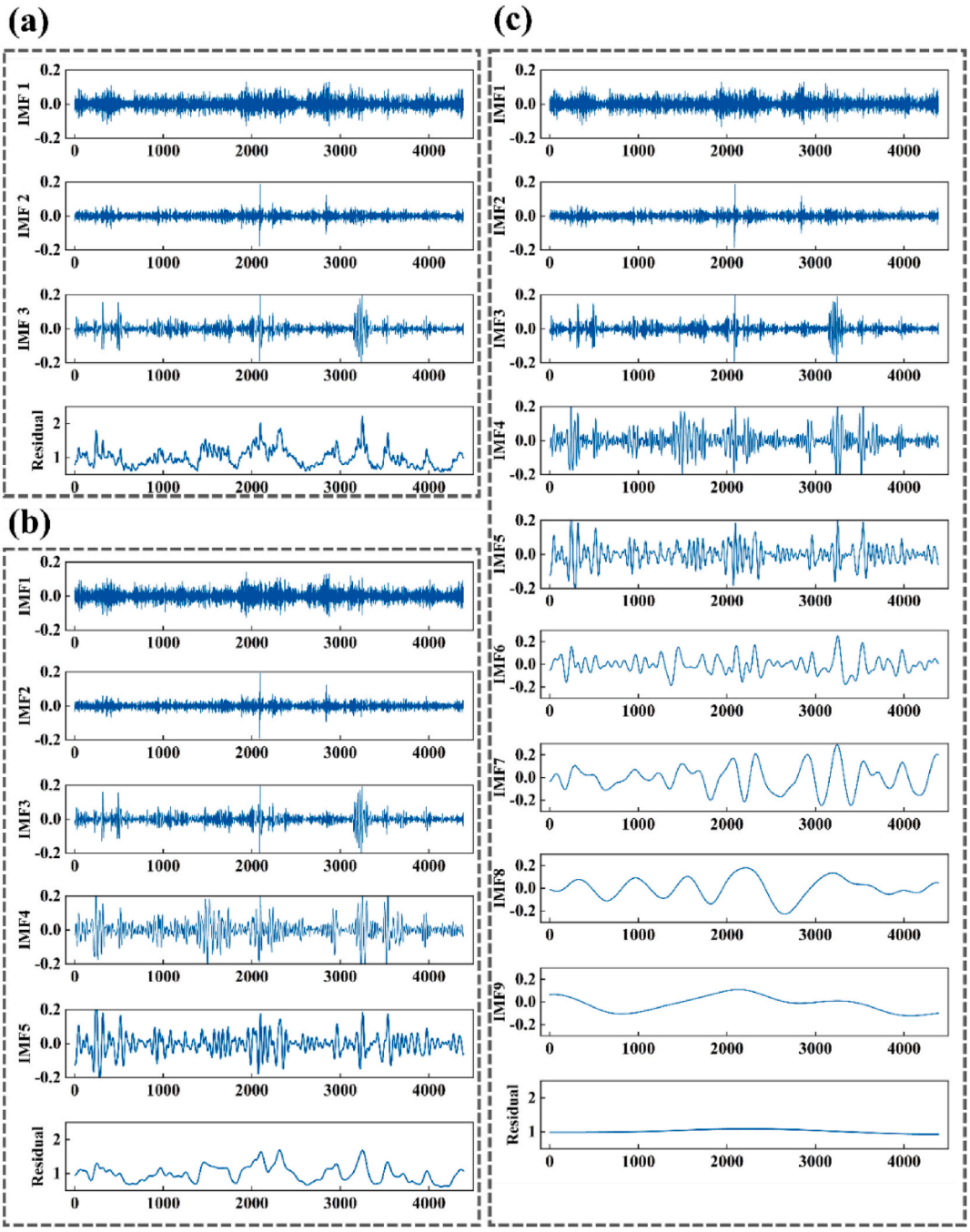

Fig. 11. Decomposed signals with the number of IMFs set to (a) 3, (b) 5, and (c) 9.

the number of IMFs does not uniformly decrease prediction error. For instance, at buoy point 46,221, the RMSE values for the EEMD-SVR model with 3, 5, 7, and 9 IMFs are 0.2431, 0.2970, 0.3148, and 0.3414, respectively, with MAE and MSE exhibiting similar trends. Similar results are observed for combinations of EEMD with EEMD-ANN and EEMD-LSTM. When too many IMFs are decomposed, excessive noise is introduced, negatively affecting the final prediction accuracy. This results in relatively larger differences in RMSE values across different numbers of IMFs.

Fig. 12 compares the prediction errors and computation times for SWH predictions using EEMD. The graph reveals that RMSE tends to increase as the number of IMFs rises. The reason for this phenomenon is that the IMF and residual sequences obtained after EEMD decomposition exhibit certain stability and periodicity, and their changing characteristics can be better captured by machine learning models. However, excessive IMF decomposition does not improve the predictability of the IMFs, as the higher order time series in Fig. 11 still show uncertainties, and decomposition of white-noise-involved time series may cause additional error. Notably, the order of performance from most to least accurate is: EEMD-ANN, EEMD-LSTM, and EEMD-SVR, which aligns with the observations made in Section 3.1. This indicates that for time series prediction with a limited training sample size, LSTM models may underperform due to underfitting—a finding that has not been previously reported. Additionally, the computational runtime for predicting SWH using varying numbers of IMFs across different machine learning models is charted on the right axis of Fig. 12. As the number of decomposed IMFs and model complexity increases, the running time also increases. Therefore, it is crucial to select an optimal number of

Table 3
Errors of different prediction methods with various numbers of decomposed IMFs and different continuous prediction step lengths.

Station	Number of IMFs	Steps	EEMD-SVR			EEMD-ANN			EEMD-LSTM		
			RMSE	MAE	MSE	RMSE	MAE	MSE	RMSE	MAE	MSE
46,221	3	12	0.2431	0.1673	0.0591	0.2149	0.1260	0.0462	0.2381	0.1494	0.0567
		24	0.3727	0.2497	0.1389	0.2659	0.1661	0.0707	0.3053	0.1999	0.0932
		48	0.5629	0.3720	0.3168	0.3250	0.2032	0.1056	0.3411	0.2121	0.1164
	5	12	0.2970	0.2101	0.0882	0.2269	0.1342	0.0515	0.2547	0.1618	0.0649
	7	12	0.3148	0.2403	0.0991	0.2361	0.1482	0.0558	0.2567	0.1654	0.0659
	9	12	0.3414	0.2694	0.1166	0.2505	0.1625	0.0627	0.2849	0.2030	0.0811
46,251	3	12	0.2758	0.1942	0.0761	0.2478	0.1563	0.0614	0.2604	0.1648	0.0678
		24	0.3935	0.2796	0.1549	0.3061	0.2081	0.0937	0.3416	0.2408	0.1167
		48	0.5528	0.3915	0.3056	0.3672	0.2472	0.1348	0.3921	0.2585	0.1537
	5	12	0.3225	0.2326	0.1040	0.2641	0.1677	0.0697	0.3002	0.1915	0.0901
	7	12	0.3350	0.2545	0.1122	0.2797	0.1867	0.0782	0.3053	0.2075	0.0932
	9	12	0.4079	0.3296	0.1664	0.3002	0.2035	0.0901	0.3444	0.2503	0.1186

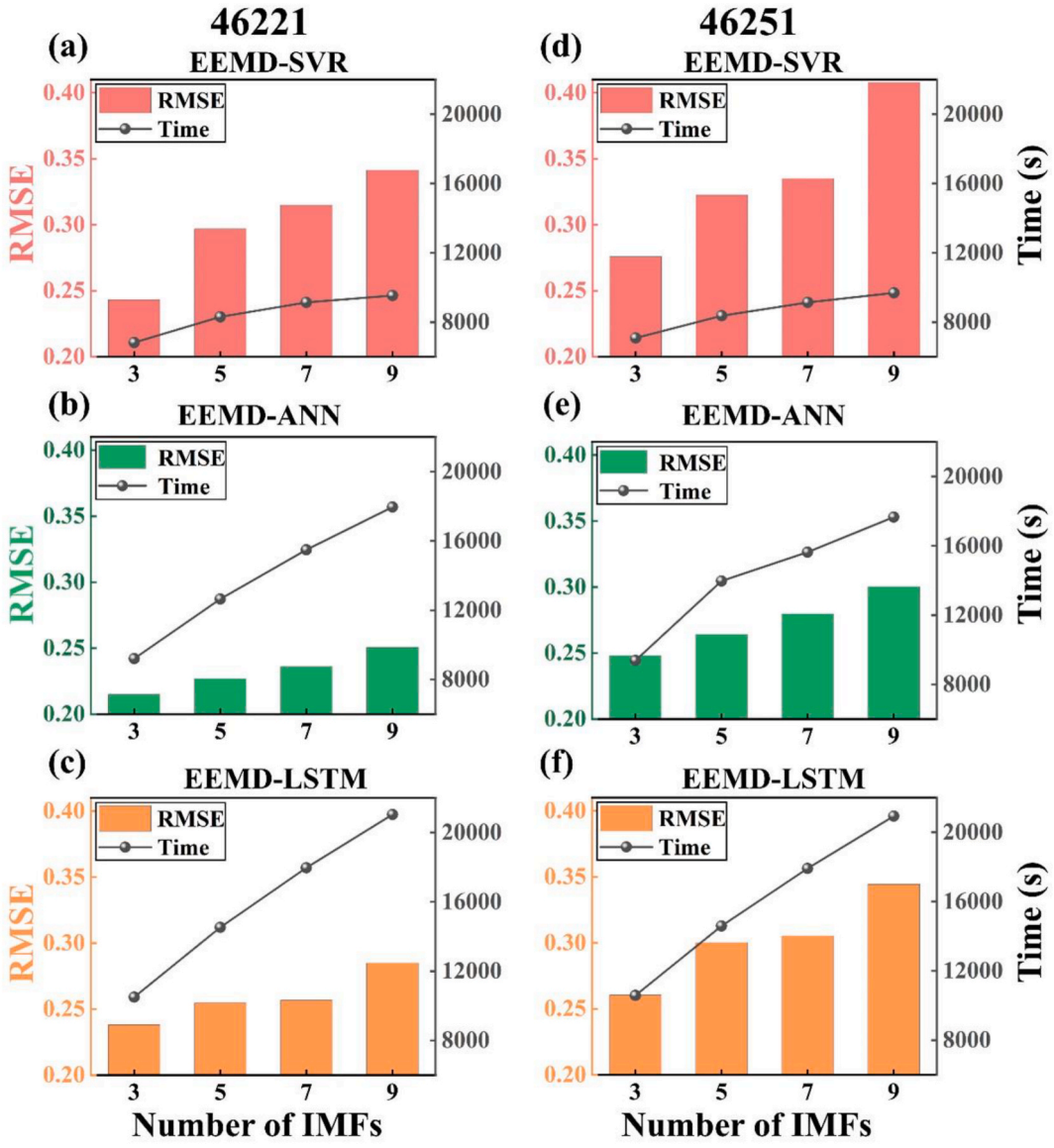

Fig. 12. At buoy 46,221, bar charts of prediction RMSE and line charts of consumed time for different numbers of decomposed IMFs using (a)EEMD-SVR, (b)EEMD-ANN, and (c)EEMD-LSTM; at buoy 46,251, bar charts of prediction RMSE and line charts of consumed time for different numbers of decomposed IMFs using (d) EEMD-SVR, (e)EEMD-ANN, and (f) EEMD-LSTM.

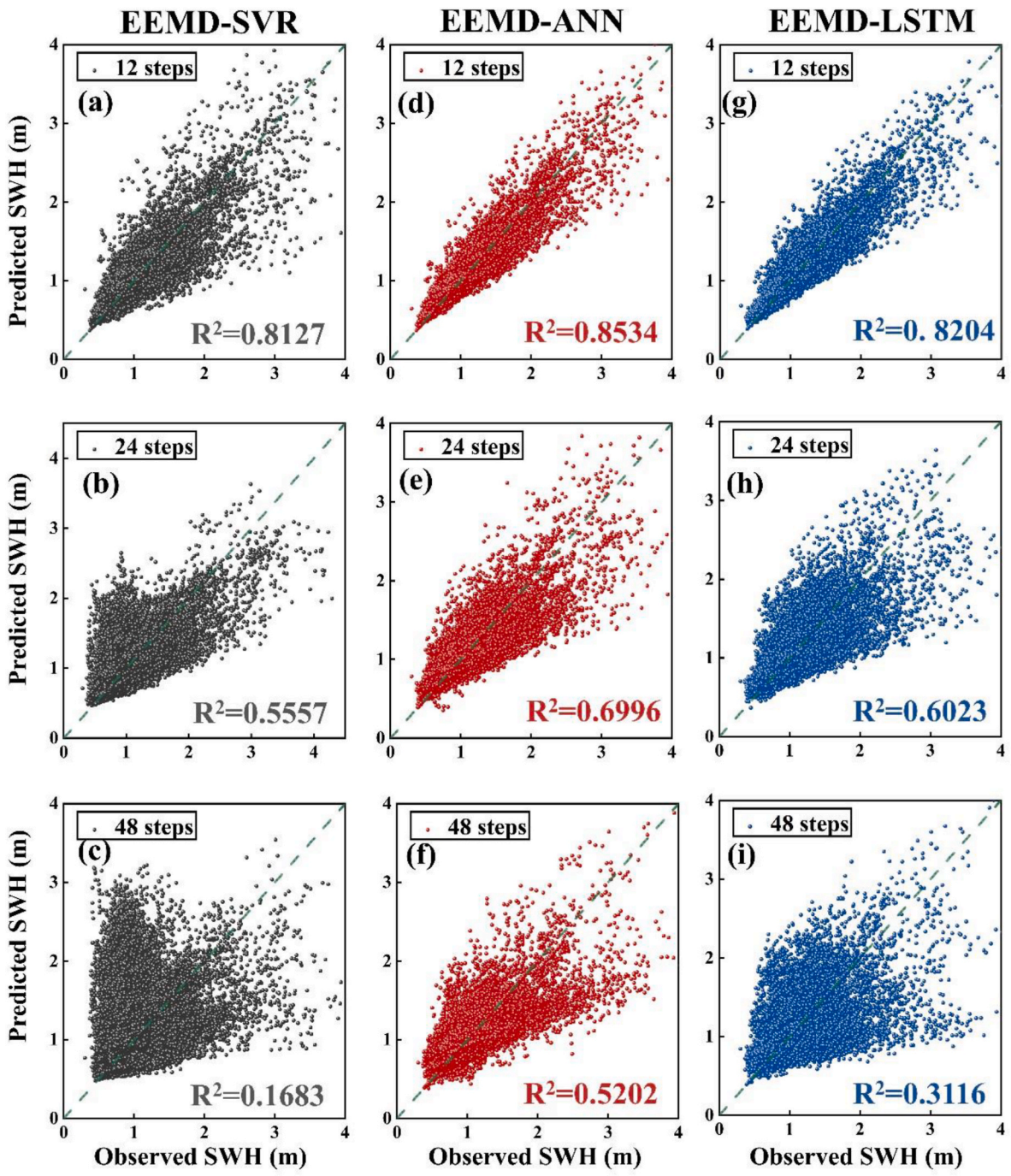

Fig. 13. Scatter plots of (a) 12-step, (b) 24-step, and (c) 48-step continuous predictions using EEMD-SVR at buoy 46,221; scatter plots of (d) 12-step, (e) 24-step, and (f) 48-step continuous predictions using EEMD-ANN; scatter plots of (g) 12-step, (h) 24-step, and (i) 48-step continuous predictions using EEMD-LSTM.

IMFs to effectively balance prediction accuracy and computational efficiency.

Therefore, the selection of IMFs in the EEMD model significantly influences both prediction errors and computation time in forecasting SWH. This highlights the importance of thoroughly evaluating the optimal number of IMFs for practical applications, a discussion that has not been extensively covered in previous research.

3.3. Impact of different continuous prediction step lengths on accuracy of SWH prediction

The ability of a model to predict SWH continuously over extended periods is crucial. Table 3 details the prediction errors for different models—EEMD-SVR, EEMD-ANN, and EEMD-LSTM—across continuous prediction lengths of 12 steps (12 h), 24 steps (24 h), and 48 steps (48 h), with each using 3 decomposed IMFs. The data reveal that error rates for all the methods increase with longer prediction intervals. For instance, at buoy point 46,221, the RMSE for a 12-step forecast using EEMD-SVR is 0.2431, but this escalates to 0.3727 and 0.5629, i.e., an increase of 53% and 132%, respectively, for 24-step and 48-step forecasts. Similarly, MAE and MSE show comparable increasing trends, with MAE increasing by 49% and 122%, and MSE increasing by 135% and 436%, respectively. This pattern of increasing errors with longer forecast intervals is consistent across different prediction models and also observed at buoy point 46,251, hence suggesting a general trend of accuracy degradation with extended prediction lengths. In other words, excessive

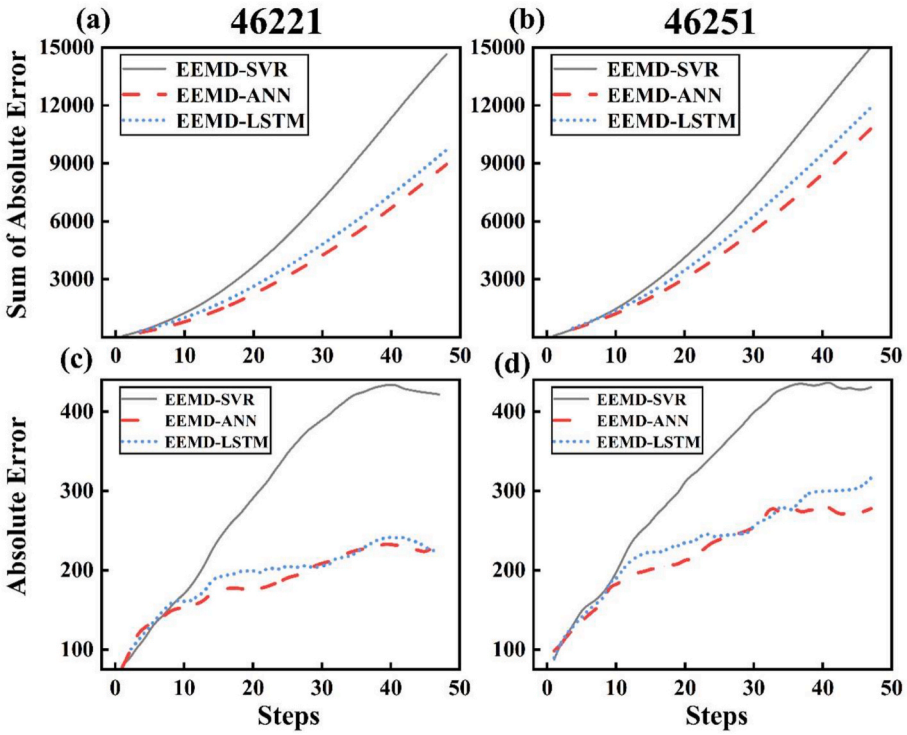

Fig. 14. The cumulative error plot of 48-step continuous predictions for buoy (a) 46,221 and buoy (b) 46,251, and the single-step absolute error plot of 48-step continuous predictions for buoy (c) 46,221 and buoy (d) 46,251.

continuous prediction step lengths lead to a rapid decline in the accuracy of hybrid prediction methods due to the cumulative effect of prediction errors.

To illustrate the above, Fig. 13 provides a visual comparison of scatter plots for the hybrid prediction methods at buoy point 46,221, considering different continuous prediction step lengths. The results show that as the prediction step length increases, the prediction errors of the three hybrid models grow significantly, and the predictions deviate more noticeably from the measured data.

To further explore this trend, Fig. 14 presents error accumulation curves across various prediction steps. Fig. 14(a) and (b) track the absolute errors at each prediction step and their cumulative totals over a 48-step forecast, while Fig. 14(c) and (d) displays the total accumulated errors at each step within the same forecast period. The first ten prediction steps show a relatively steady increase in errors, but beyond this point, the error growth curves steepen noticeably. This pattern highlights a significant decline in prediction accuracy as the forecast period extends, demonstrating the cumulative impact of prediction errors over time. As the number of prediction steps increases, the rapid escalation of errors suggests that the model may have inherent limitations. This phenomenon emphasizes the challenges of maintaining accuracy in long-term SWH forecasting and underscores the need for models that are better calibrated for longer-term predictions.

Additionally, the prediction accuracy of different hybrid prediction methods varies with different continuous prediction step lengths. Fig. 15 (a–f) show the violin plots of absolute errors for the three different hybrid prediction methods. Notably, the error accumulation in the EEMD-ANN method increases at a slower rate compared to EEMD-SVR and EEMD-LSTM, a trend also observable in Fig. 14(a–d). This discrepancy may stem from the differing capabilities of the models to process noisy data. Specifically, the LSTM model, despite its robust learning capabilities, might be more prone to interference from white noise, leading to misinterpretations of the wave height variation process. Conversely, the SVR model, with its less potent learning capacity, may not effectively capture the true trends in wave height variations. Meanwhile, the ANN model demonstrates a relatively superior ability to accurately track these variations. As the number of continuous prediction steps increases, the prediction error rises rapidly. The ability of existing methods to handle continuous predictions needs improvement, and new models are required to address the challenges of long-term predictions.

Fig. 15(g) presents a comparison of the time efficiency of these hybrid models at varying prediction lengths. It reveals that the time required for predictions decreases as the prediction interval extends. Additionally, the LSTM model consumes more time than the ANN, which in turn requires more time than the SVR model. This pattern is attributed to the need for repeating the EEMD, model training, and prediction processes after each prediction cycle. As the length of continuous prediction steps increases, fewer cycles of EEMD and model training are necessary, thereby speeding up the overall prediction process. Furthermore, the complexity of the LSTM model necessitates longer training periods compared to the simpler ANN and SVR models, contributing to its longer time consumption.

4. Conclusion

Accurate prediction of Significant Wave Height (SWH) is vital for marine engineering and safe navigation. This study integrates Ensemble Empirical Mode Decomposition (EEMD) with three distinct predictive models—Support Vector Regression (SVR), Artificial Neural Networks (ANN), and Long Short-Term Memory Networks (LSTM). The comparison of model performance across different key factors such as the number of decomposed Intrinsic Mode Functions (IMFs) and various forecasting durations are presented in detailed. The main conclusions from this comprehensive analysis are below:

(1) The prediction accuracy is notably enhanced by employing EEMD. For instance, at buoy point 46,221, the RMSE reduces 25% for SVR, 15% for ANN, and 8% for LSTM. When using EEMD, the complexity of the predictive model should be considered, as

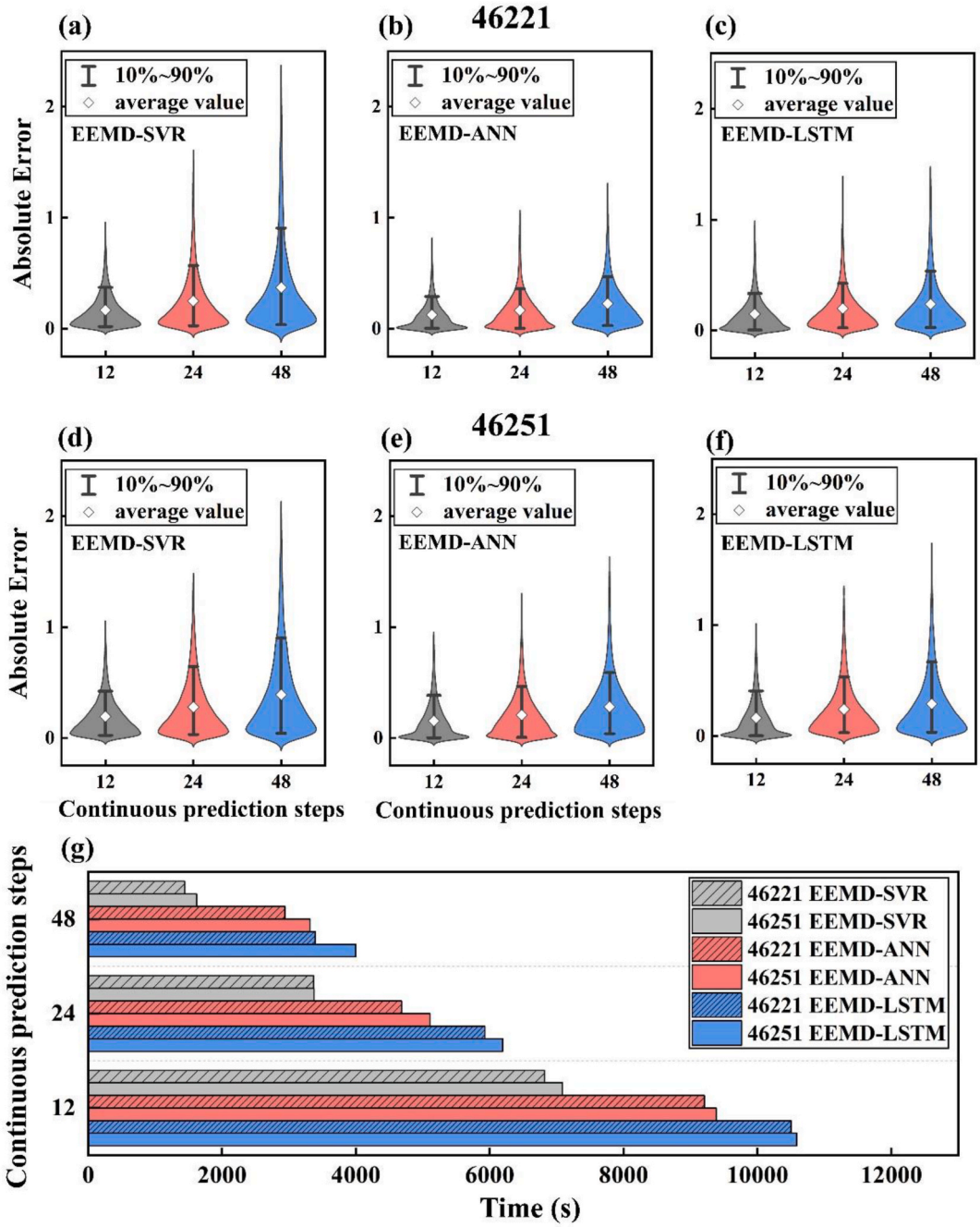

Fig. 15. Box plots of cumulative absolute errors for different continuous prediction steps at Buoy 46,221 using EEMD-SVR (a), EEMD-ANN (b), and EEMD-LSTM (c), and at Buoy 46,251 using EEMD-SVR (d), EEMD-ANN (e), and EEMD-LSTM (f), as well as (g) the comparison of time consumption for different prediction methods at different continuous prediction steps.

the reduction in information content after EEMD decomposition can lead to underfitting issues, RMSE for EEMD-ANN model is smaller than EEMD-LSTM, Moreover, the accuracy fluctuates seasonally, with higher errors during periods of significant SWH variation. More stable conditions yield better accuracy.

(2) The quantity of IMFs decomposed by EEMD is a critical parameter influencing the prediction accuracy. However, increasing the number of IMFs does not consistently decrease the prediction error. For example, at buoy point 46,221, using EEMD-ANN for continuous 12-step prediction, the RMSE is 0.2149 when the number of IMFs decompositions is 3; when the number of IMFs decompositions is increased to 9, the RMSE increases to 0.2505. Excessive decomposition is found to reduced accuracy and increased prediction time.

(3) Increasing the continuous prediction step length results in higher prediction errors due to cumulative error effects, leading to diminished accuracy over time. Moreover, the prediction error increases linearly for continuous prediction. Among the tested models, the ANN displayed the slowest error accumulation. The results demonstrate a potential to for proposing a new model for long-term continuous prediction.

In all, these findings underscore the importance of optimizing EEMD parameters and selecting appropriate machine learning models to effectively predict SWH. In the future, these findings are expected to

enhance the reliability and efficiency of wave prediction systems, thereby playing an important role in maritime safety and ocean engineering management.

CRediT authorship contribution statement

Yuanye Guo: Writing – review & editing, Writing – original draft, Visualization, Validation, Software, Methodology, Investigation, Formal analysis, Data curation, Conceptualization. **Jicang Si:** Writing – review & editing, Supervision, Resources, Conceptualization. **Yulian Wang:** Writing – review & editing, Investigation. **Farhan Hanif:** Writing – review & editing. **Shuang Li:** Writing – review & editing. **Mengwei Wu:** Writing – review & editing. **Minyi Xu:** Writing – review & editing, Supervision, Resources, Funding acquisition. **Jianchun Mi:** Writing – review & editing, Supervision, Resources.

Declaration of competing interest

The authors declare that they have no known competing financial interests or personal relationships that could have appeared to influence the work reported in this paper.

Acknowledgement

The authors greatly acknowledge the support of the Application Research Program of Liaoning Province (Grant No. 2022JH2/101300219), the Fundamental Research Funds for the Central Universities (No. 3132024218), and the support by high-performance computing platform of Peking University.

References

Agrawal, J., Deo, M., 2002. On-line wave prediction. Mar. Struct. 15 (1), 57–74.
Altunkaynak, A., Çelik, A., Mandev, M.B., 2023. Hourly significant wave height prediction via singular spectrum analysis and wavelet transform based models. Ocean. Eng. 281, 114771.
Booij, N., Ris, R.C., Holthuijsen, L.H., 1999. A third-generation wave model for coastal regions: 1. Model description and validation. J. Geophys. Res.: Oceans 104 (C4), 7649–7666.
Cornejo-Bueno, L., Garrido-Merchán, E.C., Hernández-Lobato, D., Salcedo-Sanz, S., 2018. Bayesian optimization of a hybrid system for robust ocean wave features prediction. Neurocomputing 275, 818–828.
Cortes, C., Vapnik, V., 1995. Support-vector networks. Mach. Learn. 20, 273–297.
Deo, M., Jagdale, S., 2003. Prediction of breaking waves with neural networks. Ocean. Eng. 30 (9), 1163–1178.
Deo, M., Naidu, C.S., 1998. Real time wave forecasting using neural networks. Ocean. Eng. 26 (3), 191–203.
Ding, J., Deng, F., Liu, Q., Wang, J., 2023. Regional forecasting of significant wave height and mean wave period using EOF-EEMD-SCINet hybrid model. Appl. Ocean Res. 136, 103582.
Drucker, H., Burges, C.J., Kaufman, L., Smola, A., Vapnik, V., 1996. Support vector regression machines. Adv. Neural Inf. Process. Syst. 9.
Duan, W.-y., Huang, L.-m., Han, Y., Huang, D.-t., 2016a. A hybrid EMD-AR model for nonlinear and non-stationary wave forecasting. J. Zhejiang Univ. - Sci. A. 17 (2), 115–129.
Duan, W., Han, Y., Huang, L., Zhao, B., Wang, M., 2016b. A hybrid EMD-SVR model for the short-term prediction of significant wave height. Ocean. Eng. 124, 54–73.
Fan, G., Yu, P., Wang, Q., Dong, Y., 2023. Short-term motion prediction of a semi-submersible by combining LSTM neural network and different signal decomposition methods. Ocean Eng. 267, 113266.
Fan, S., Xiao, N., Dong, S., 2020. A novel model to predict significant wave height based on long short-term memory network. Ocean. Eng. 205, 107298.
Gaur, S., Deo, M., 2008. Real-time wave forecasting using genetic programming. Ocean. Eng. 35 (11–12), 1166–1172.
Graham, C., 1982. The parameterisation and prediction of wave height and wind speed persistence statistics for oil industry operational planning purposes. Coast. Eng. 6 (4), 303–329.
Group, T.W., 1988. The WAM model—a third generation ocean wave prediction model. J. Phys. Oceanogr. 18 (12), 1775–1810.
Hanif, M.F., Naveed, M.S., Metwaly, M., Si, J., Liu, X., Mi, J., 2024a. Advancing solar energy forecasting with modified ANN and light GBM learning algorithms. AIMS Energy 12 (2), 350–386.
Hanif, M.F., Siddique, M.U., Si, J., Naveed, M.S., Liu, X., Mi, J., 2024b. Enhancing solar forecasting accuracy with sequential deep artificial neural network and hybrid random forest and gradient boosting models across varied terrains. Adv. Theory Simul., 2301289
Hao, W., Sun, X., Wang, C., Chen, H., Huang, L., 2022. A hybrid EMD-LSTM model for non-stationary wave prediction in offshore China. Ocean. Eng. 246, 110566.
Haver, S., 1986. A Wave Climate Description for Long-Term Response Calculations, vol. 86. Proc. OMAE', pp. 27–34.
Hochreiter, S., Schmidhuber, J., 1997. Long short-term memory. Neural Comput. 9 (8), 1735–1780.
Holthuijsen, L., Booij, N., Herbers, T., 1989. A prediction model for stationary, short-crested waves in shallow water with ambient currents. Coast. Eng. 13 (1), 23–54.
Holthuijsen, L.H., 2010. Waves in Oceanic and Coastal Waters. Cambridge Univ. Press.
Huang, N.E., Shen, Z., Long, S.R., Wu, M.C., Shih, H.H., Zheng, Q., Yen, N.-C., Tung, C.C., Liu, H.H., 1998. The empirical mode decomposition and the Hilbert spectrum for nonlinear and non-stationary time series analysis. Proc. R. Soc. Lond. A: Math. Phys. Eng. Sci. 454 (1971), 903–995.
Jain, P., Deo, M., 2006. Neural networks in ocean engineering. Ships Offshore Struct. 1 (1), 25–35.
Janssen, P.A., 2008. Progress in ocean wave forecasting. J. Comput. Phys. 227 (7), 3572–3594.
Kingma, D., 2014. Adam: a method for stochastic optimization. arXiv preprint arXiv: 1412.6980, 2014.
Komen, G., Hasselmann, S., Hasselmann, K., 1984. On the existence of a fully developed wind-sea spectrum. J. Phys. Oceanogr. 14 (8), 1271–1285.
Komen, G.J., Cavaleri, L., Donelan, M., Hasselmann, K., Hasselmann, S., Janssen, P., 1996. Dynamics and Modelling of Ocean Waves.
LeCun, Y., Bottou, L., Bengio, Y., Haffner, P., 1998. Gradient-based learning applied to document recognition. Proc. IEEE 86 (11), 2278–2324.
Liu, X., Huang, W., Gill, E.W., 2017. Estimation of significant wave height from X-band marine radar images based on ensemble empirical mode decomposition. Geosci. Rem. Sens. Lett. IEEE 14 (10), 1740–1744.
Mahjoobi, J., Etemad-Shahidi, A., Kazeminezhad, M., 2008. Hindcasting of wave parameters using different soft computing methods. Appl. Ocean Res. 30 (1), 28–36.
Mahjoobi, J., Mosabbeb, E.A., 2009. Prediction of significant wave height using regressive support vector machines. Ocean. Eng. 36 (5), 339–347.
Makarynskyy, O., 2004. Improving wave predictions with artificial neural networks. Ocean. Eng. 31 (5–6), 709–724.
Malekmohamadi, I., Bazargan-Lari, M.R., Kerachian, R., Nikoo, M.R., Fallahnia, M., 2011. Evaluating the efficacy of SVMs, BNs, ANNs and ANFIS in wave height prediction. Ocean. Eng. 38 (2–3), 487–497.
McCulloch, W.S., Pitts, W., 1943. A logical calculus of the ideas immanent in nervous activity. Bull. Math. Biophys. 5, 115–133.
Özger, M., Altunkaynak, A., Şen, Z., 2004. Statistical investigation of expected wave energy and its reliability. Energy Convers. Manag. 45 (13–14), 2173–2185.
Ramsey, F.L., 1974. Characterization of the partial autocorrelation function. Ann. Stat. 1296–1301.
Rasp, S., Dueben, P.D., Scher, S., Weyn, J.A., Mouatadid, S., Thuerey, N., 2020. WeatherBench: a benchmark data set for data-driven weather forecasting. J. Adv. Model. Earth Syst. 12 (11), e2020MS002203.
Richter, M., Schaut, S., Walser, D., Schneider, K., Sawodny, O., 2017. Experimental validation of an active heave compensation system: estimation, prediction and control. Control Eng. Pract. 66, 1–12.
Rilling, G., Flandrin, P., Gonçalves, P., Lilly, J.M., 2007. Bivariate empirical mode decomposition. IEEE Signal Process. Lett. 14 (12), 936–939.
Sadeghifar, T., Nouri Motlagh, M., Torabi Azad, M., Mohammad Mahdizadeh, M., 2017. Coastal wave height prediction using recurrent Neural Networks (RNNs) in the South Caspian Sea. Mar. Geod. 40 (6), 454–465.
Soares, C.G., Ferreira, A., Cunha, C., 1996. Linear models of the time series of significant wave height on the Southwest Coast of Portugal. Coast. Eng. 29 (1–2), 149–167.
Song, T., Wang, J., Huo, J., Wei, W., Han, R., Xu, D., Meng, F., 2023. Prediction of significant wave height based on EEMD and deep learning. Front. Mar. Sci. 10, 1089357.
Taylor, J.W., Jeon, J., 2018. Probabilistic forecasting of wave height for offshore wind turbine maintenance. Eur. J. Oper. Res. 267 (3), 877–890.
Tolman, H.L., Balasubramaniyan, B., Burroughs, L.D., Chalikov, D.V., Chao, Y.Y., Chen, H.S., Gerald, V.M., 2002. Development and implementation of wind-generated ocean surface wave Modelsat NCEP. Weather Forecast. 17 (2), 311–333.
Torres, M.E., Colominas, M.A., Schlotthauer, G., Flandrin, P., 2011. A complete ensemble empirical mode decomposition with adaptive noise. In: 2011 IEEE International Conference on Acoustics, Speech and Signal Processing (ICASSP). IEEE, pp. 4144–4147.
Wang, W., Tang, R., Li, C., Liu, P., Luo, L., 2018. A BP neural network model optimized by mind evolutionary algorithm for predicting the ocean wave heights. Ocean. Eng. 162, 98–107.
Wu, Z., Huang, N.E., 2005. Statistical significance test of intrinsic mode functions, Hilbert-Huang Transform and its applications. World Sci. 107–127.
Wu, Z., Huang, N.E., 2009. Ensemble empirical mode decomposition: a noise-assisted data analysis method. Adv. Adapt. Data Anal. 1 (1), 1–41.
Wu, Z., Huang, N.E., 2010. On the filtering properties of the empirical mode decomposition. Adv. Adapt. Data Anal. 2 (4), 397–414.
Yeh, J.-R., Shieh, J.-S., Huang, N.E., 2010. Complementary ensemble empirical mode decomposition: a novel noise enhanced data analysis method. Adv. Adapt. Data Anal. 2 (2), 135–156.